

Operation and performance of the upgraded ALICE Inner Tracking System

Jian Liu^{a,*} for the ALICE Collaboration

^a*University of Liverpool,*

Department of Physics, Liverpool, United Kingdom

E-mail: j.1.liu@liverpool.ac.uk

The ALICE detector underwent significant upgrades during the LHC Long Shutdown 2 from 2019 to 2021. A key upgrade was the installation of the new Inner Tracking System (ITS2), comprising 7 layers with 12.5 billion pixels over 10 m², enhancing its tracking capabilities using the ALPIDE chips that are capable of recording Pb–Pb collisions at an interaction rate of 50 kHz. ITS2 offers a significant improvement in impact parameter resolution and tracking efficiency at low transverse momentum, attributed to its increased granularity, low material budget of only 0.36% X_0 /layer for the innermost 3 layers and the closer positioning of the first layer to the interaction point.

ITS2 was successfully installed and commissioned in ALICE, becoming operational with the start of LHC Run 3. This paper provides an overview of its operation and initial performance results, focusing on calibration, tracking performance in both pp and Pb–Pb collisions, and studies on particle identification.

42nd International Conference on High Energy Physics (ICHEP2024)

18-24 July 2024

Prague, Czech Republic

*Speaker

1. Introduction

The ALICE experiment [1] at the LHC is designed to explore heavy-ion physics, focusing on quark–gluon plasma and strongly interacting matter at extreme energy densities. By analyzing various collisions, including nucleus–nucleus, proton–proton and proton–nucleus, ALICE studies the properties of this high-density matter. A key challenge of ALICE is reconstructing tracks in the high multiplicity environment of central Pb–Pb collisions while providing comprehensive particle identification across a wide transverse momentum range. To extend its physics reach, ALICE underwent major upgrades during Long Shutdown 2 (LS2) from 2019 to 2021 [2], improving tracking precision, particularly for low transverse momentum particles.

A major component of these upgrades was the implementation of the new Inner Tracking System (ITS2), enhancing impact parameter resolution and tracking performance. The system architecture is outlined in Section 2, with calibration and performance details discussed in Sections 3 and 4.

2. Detector system architecture

The ITS2 [3] is a seven-layer silicon pixel detector that utilizes Monolithic Active Pixel Sensors (MAPS) technology, specifically the ALPIDE sensor [4]. ITS2 covers an area of 10 m^2 and is composed of an inner barrel (IB) with three layers and an outer barrel (OB) with four layers, totaling 192 staves. Each ALPIDE sensor consists of 512×1024 pixels with a pixel pitch of $27 \mu\text{m} \times 29 \mu\text{m}$, providing a spatial resolution of approximately $5 \mu\text{m}$. The reduced chip thickness ($50 \mu\text{m}$ for the IB and $100 \mu\text{m}$ for the OB), combined with lightweight mechanical supports, reduces the material budget to $0.36\% X_0/\text{layer}$ in the inner barrel. A detailed description of the detector geometry is available in [2].

Figure 1 outlines the detector control and readout systems. The Detector Control System (DCS) manages communication with the detector via the Common Readout Unit (CRU) and the Readout Unit (RU). DCS handles the control of the detector itself and its infrastructure, including the RUs, power boards, and the cooling system. The DCS monitors over 100,000 data points, archives data, and enables automatic recovery during runs to maximize detector efficiency and acceptance. An independent safety system interlocks the CAEN power channels based on stave temperatures and the status of the cooling plant loop.

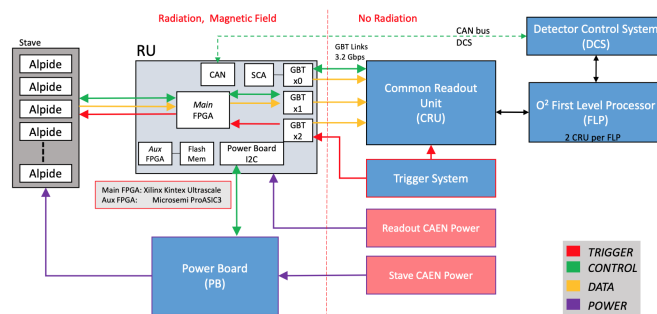


Figure 1: Diagram of the detector control and readout systems.

Frame data from the matrix is read out using zero-suppression, implemented through priority encoders. The data is transmitted serially using differential signaling at speeds of up to 1.2 Gbps with 8b/10b encoding, achieving a maximum effective throughput of 960 Mbps. To maintain modularity, the readout electronics are organized into 192 autonomous units, each managing a stave, and located in a radiation environment. The main FPGA on the RU handles detector control, data packaging, and prepares the data stream for conversion through the versatile link. Radiation effects are mitigated through techniques such as scrubbing and triple modular redundancy.

Detector data from the staves is packaged at the RUs, aggregated at the CRUs on the First Level Processors, and then sent to the Event Processing Nodes for both synchronous and asynchronous reconstruction. Quality control and calibration tasks run in both modes to monitor data integrity, detector occupancy, pixel charge thresholds, and reconstruction performance.

3. Calibration

Calibrating the ITS2 is crucial for ensuring stable operation and high data quality, particularly given the complexity of managing its 12.5 billion pixels. The calibration involves two main steps: tuning pixel charge thresholds and masking noisy pixels, both of which are vital for achieving uniform detector response and optimizing tracking efficiency during data collection.

The threshold of each ALPIDE sensor is adjusted globally using two on-chip Digital-to-Analog Converters (DACs). To achieve the target threshold, a test pulse is applied to the pixel matrix, allowing the DAC settings to be fine-tuned until the desired value is reached.

Following the threshold tuning, scans are performed on approximately 2% of pixels per chip, evenly distributed across the matrix, and lasting about 5 minutes during LHC beam dump periods to verify the threshold distribution across the detector. During longer no-beam periods, such as LHC

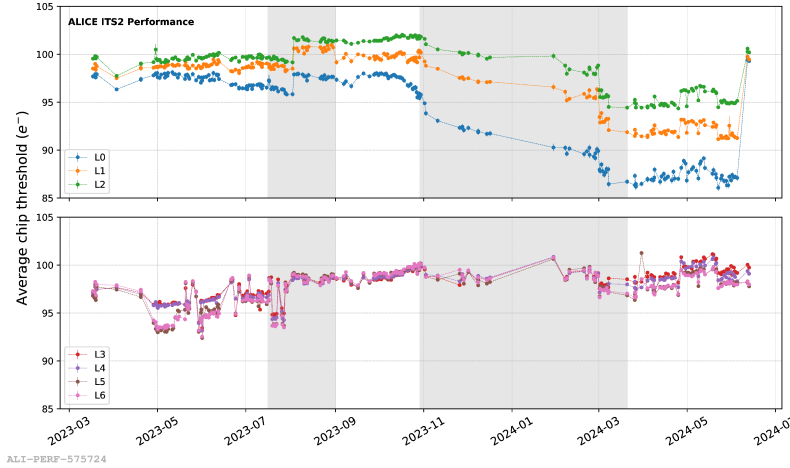


Figure 2: Average threshold evolution per layer. The grey background indicates no-beam periods. Variations in May, July, and August 2023 were due to power supply optimizations for the ALPIDE sensors. The IB was retuned to 100 electrons in June 2024, as shown in the final point of the top plot.

technical stops, full pixel matrix scans are conducted. As shown in Figure 2, the average threshold variation per layer remained within 15 electrons during the early phase of Run 3, demonstrating

stability. Minor fluctuations were linked to power supply optimizations. In 2023, a decrease in threshold was observed on IB after Pb–Pb runs, consistent with previous irradiation studies conducted during sensor R&D. This was compensated in June 2024 with a retuning, restoring the target threshold of 100 electrons.

After pixel threshold calibration, a noise scan is conducted to identify and mask noisy pixels. Pixels with an occupancy above 10^{-2} hits/event in the IB and 10^{-6} hits/event in the OB are flagged and masked during data collection. The relaxed threshold in the IB optimizes detection efficiency while keeping the readout bandwidth and reconstruction load manageable. At the nominal threshold of 100 electrons, only a few tens of pixels per chip are masked, resulting in a fake-hit rate (FHR) of approximately 10^{-8} hits/event/pixel, well below the requirement of 10^{-6} hits/event/pixel. Overall, only 0.004% of pixels across the detector are masked. As shown in Figure 3, the average FHR per

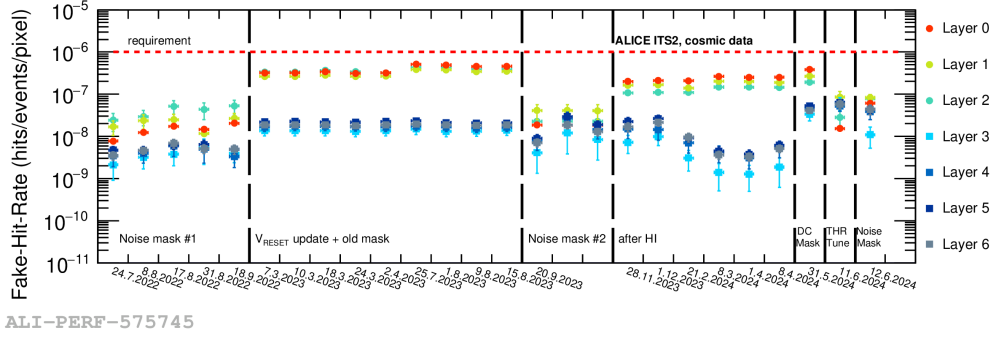


Figure 3: Average FHR per layer after noisy pixel masking.

layer remains stable over time, with no significant changes in noisy pixel locations despite radiation exposure during Run 3. This stability allows the detector to operate effectively with static noise masks, removing the need for recalibration during data-taking.

4. Performance

Since the start of Run 3, the ITS2 has been actively collecting physics data from pp collisions at $\sqrt{s} = 13.6$ TeV, primarily at an inelastic interaction rate of 650 kHz, and from Pb–Pb collisions at $\sqrt{s_{NN}} = 5.36$ TeV, with peak rates so far reaching 47 kHz.

The impact parameter resolution for reconstructed global tracks in pp and Pb–Pb collisions, where ITS standalone tracks are matched with those reconstructed in the TPC, is shown in Figure 4. A two-fold improvement is observed in the $r\phi$ plane compared to Run 2, bringing the results close to the expected values. There is a remaining 20% discrepancy between the data and Monte Carlo simulations which is attributed to residual misalignment and a potentially too coarse description of the detector material in simulations.

The reduced distance between the primary vertex and the innermost layers (2.2 to 4 cm) allows tracking of charged weakly decaying particles before their decay, using the strangeness tracking algorithm. By leveraging the proximity of the first layer to the primary vertex, this method directly detects hits from weakly decaying hadrons before they decay, combining this information

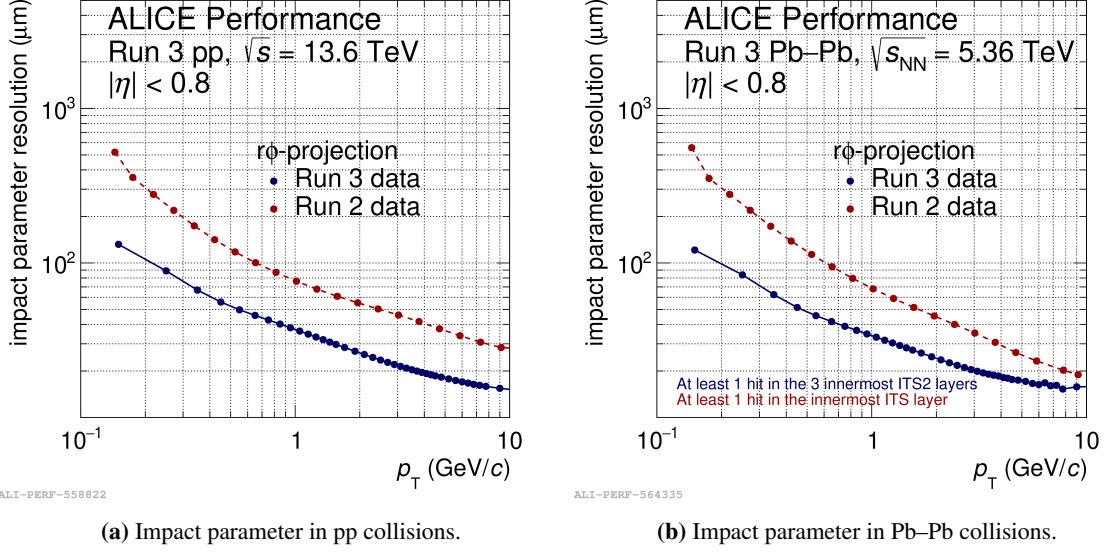


Figure 4: Impact parameter in $r\phi$ plane based on ITS–TPC global tracks.

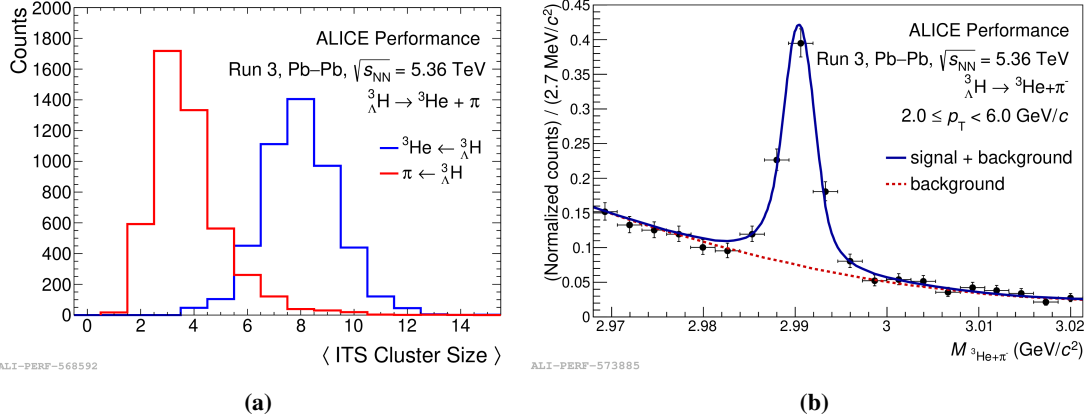


Figure 5: PID for hypernuclei and heavy-ionising particles. (a) The average ITS2 cluster size of hypertriton daughter tracks. (b) The invariant mass of the sum of hypertriton and antihypertriton.

with their decay products to significantly improve the pointing resolution. This capability enables high-resolution studies of non-prompt cascades, hypernuclei, and exotic bound states.

While the ALPIDE chip’s binary readout typically does not support Time over Threshold (ToT) or Particle Identification (PID) in standard operations, ITS2 can identify heavily ionizing particles (e.g., light nuclei) by analyzing their cluster size. This capability, initially proposed in the technical design report [3], has been confirmed through preliminary studies using ALICE Run 3 data. Figure 5a shows the average ITS2 cluster size of hypertriton daughter tracks (${}^3\text{He}$ and pions) measured in Pb–Pb collisions at $\sqrt{s_{NN}} = 5.36$ TeV, recorded with the standard ITS2 setting in 2023. This method uses ITS2 cluster size to tag ${}^3\text{He}$ daughter tracks and to reduce ITS–TPC fake matching. As shown in Figure 5b, a significant peak is observed for the invariant mass of the

sum of hypertriton and antihypertriton, measured from their two-body mesonic decay.

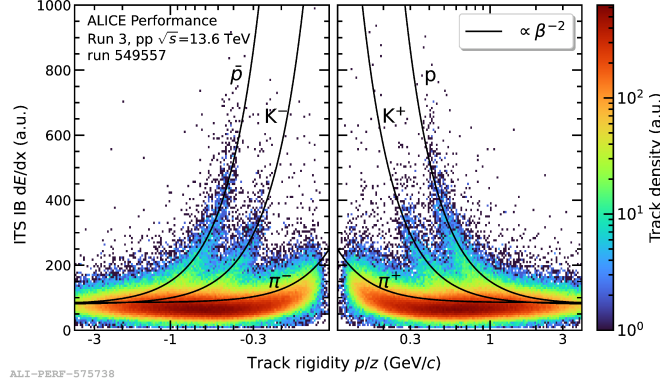


Figure 6: dE/dx spectrum measured with IB.

A proof of concept for PID was conducted using a dedicated ALPIDE setting that oversamples the sensor's analog response. Special tuning of the front-end electronics achieved a charge-proportional analog pulse length, allowing dE/dx estimation by analyzing the ToT over clusters. To minimize data loss due to oversampling, data was collected in pp collisions at around 1 kHz, the lowest interaction rate achievable at the LHC. The first dE/dx spectrum obtained is shown in Figure 6, where distinct bands for pions, kaons and protons are visible. This validates the feasibility of energy loss measurements for particle identification with thin active volume MAPS.

5. Summary

The new MAPS-based ITS2 significantly enhances ALICE's tracking capabilities, especially at low transverse momentum. Installed during LS2, ITS2 is the first MAPS detector at the LHC and has been operational since the start of Run 3.

The detector has shown excellent performance in both pp and Pb-Pb collisions, maintaining uniform pixel thresholds and achieving stable, low noise levels. Its advanced design has significantly enhanced tracking precision, with an impact parameter resolution of approximately 30 μm at $p_T = 1 \text{ GeV}/c$. Additionally, ITS2 has demonstrated particle identification capabilities for heavily ionizing particles, using cluster size during standard runs and dE/dx measurements via ToT under special low-occupancy conditions.

References

- [1] The ALICE Collaboration, *The ALICE experiment at the CERN LHC*, *JINST* **3** (2008) S08002.
- [2] The ALICE Collaboration, *ALICE upgrades during the LHC Long Shutdown 2*, *JINST* **19** (2024) P05062.
- [3] The ALICE Collaboration, *Technical Design Report for the Upgrade of the ALICE Inner Tracking System*, *J. Phys. G* **41** (2014) 087002.
- [4] Gianluca Aglieri Rinella, *The ALPIDE pixel sensor chip for the upgrade of the ALICE Inner Tracking System*, *Nucl. Instrum. Methods Phys. Res. A* **845** (2017) 583 - 587.